


FAILURE ANALYSIS AROUND ORIENTED BOREHOLES USING AN ANALYTICAL MODEL IN DIFFERENT FAULTING STRESS REGIMES

Ali LAKIROUHANI¹, Sahar GHORBANNEZHAD¹,
Jurgis MEDZVIECKAS^{2*}, Romualdas KLIUKAS³

¹Department of Civil Engineering, Faculty of Engineering, University of Zanjan, Zanjan, Iran

²Department of Reinforced Concrete Structures and Geotechnics, Vilnius Gediminas Technical University,
Saulėtekio al. 11, 10223 Vilnius, Lithuania

³Department of Applied Mechanics, Vilnius Gediminas Technical University,
Saulėtekio al. 11, 10223 Vilnius, Lithuania

Received 10 October 2022; accepted 17 March 2023

Abstract. One of the most important instabilities that may occur in a borehole is shear instability caused by high compressive stress in the borehole wall. The initial estimation of the width and depth of the failure zone around the borehole is very important in the field. In inclined boreholes, the shear instability or borehole breakout is affected by the in situ stress regime, the deviation angle of the borehole, the mechanical properties of the rock and the effect of the intermediate principal stress. In this article, an analytical model based on theory of elasticity is presented to find the breakout failure area around the inclined boreholes. Mogi-Coulomb shear failure criterion is used, in which there is also the effect of the intermediate principal stress. This model examines the failure in three-dimensional elements around the borehole for different in situ stress regime. The main finding of the analysis done in this article is that not only the deviation angle of the borehole but also the in situ stress regime has a great effect on the dimensions of the breakout. Also, the plane where the deviation angle of the borehole changes, affects the dimensions of the breakout.

Keywords: strike-slip faulting stress regime, normal faulting stress regime, reverse faulting stress regime, angle of orientation, shear failure, borehole breakout.

Introduction

Drilling deep boreholes in the ground changes the local stress field around them, and this has a negative effect on the stability and performance of the borehole. A possible consequence is the failure of the borehole wall (borehole breakout) due to stress concentration. Borehole breakout occurs when the shear stress exceeds the shear strength of the rock material. In the borehole breakout, the crushed rock is separated from the borehole wall in the form of rock spalling. The in situ stresses magnitude, the mechanical properties of the rock and the borehole pressure are the parameters that affect the dimensions and extension of the breakout failure zone, besides these parameters, porosity, stress regime and pore fluid pressure also affect the breakout dimensions.

If the borehole is vertical, the breakout is created on both sides of the borehole along the minimum horizontal principal stress, i.e., where there is the highest concentra-

tion of compressive stress (Bell & Gough, 1979; Gough & Bell, 1982; Zoback et al., 1985; Lakirouhani et al., 2021). Therefore, breakout can be an indicator to determine the direction of the in situ stresses (Bell & Gough, 1979; Hickman et al., 1985; Shamir & Zoback, 1992).

On the other hand, various shapes of breakouts have been observed in laboratory studies; V-shaped, slot-shaped (wormhole) and spiral-shaped (flake-spalling) (Haimson & Herrick, 1986; Ewy & Cook, 1990; Lee & Haimson, 1993; Herrick & Haimson, 1994; Papamichos, 1999; Van den Hoek, 2001; Haimson & Lee, 2004; Cerasi et al., 2005; Papamichos et al., 2010). This is because, depending on the microstructure characteristics of the studied rocks, breakouts can develop by different mechanisms.

For example, V-shaped breakouts, which are the most common type of breakouts, are developed by shear or tensile cracks or a combination of these two mechanisms

*Corresponding author. E-mail: jurgis.medzvieckas@vilniustech.lt

(Mastin, 1984; Haimson & Herrick, 1986; Lee & Haimson, 1993; Haimson & Song, 1993, 1998; Tronvoll & Fjaer, 1994; Cuss et al., 2003). This type of breakout has been observed in limestone (Haimson & Song, 1993) (see Figure 1a).

Slot-shaped breakouts are mainly observed in sandstones with high quartz percentage and high porosity. In this type of failure, compaction bands are formed at the breakout tip, which cause the crushing of rock grains in this location, and the failure develops until it reaches stability (Klaetsch & Haimson, 2002; Haimson & Kovachik, 2003; Haimson & Lee, 2004; Cerasi et al., 2005; Haimson, 2007) (see Figure 1b).

In the spiral-shaped breakout, the borehole wall is failed in the form of shear bands, in which shear bands spiral away from the borehole wall (Papamichos, 1999; Van den Hoek, 2001; Meier et al., 2013). This type of failure has been observed in weak sandstones (see Figure 1c).

In the last two decades, various numerical studies have been carried out in relation to the failure around the borehole and the breakout formation mechanism. Numerical studies are divided into two categories; studies based on the discrete element method (Cook et al., 2004; Potyondy & Cundall, 2004; Li et al., 2006; Rahmati et al., 2021) and studies based on the finite element method (Bahrehdar & Lakirouhani, 2022; Jolfaei & Lakirouhani, 2022). Setiawan and Zimmerman (2022) presented a semi-analytical method to investigate the episodic breakout progression by means of the conformal mapping procedure, the analysis carried out by them led to a correlation between the breakout geometry and the in situ stresses. Bahrehdar and Lakirouhani (2023) investigated the effect of the eccentricity of the borehole on the breakout dimensions using the finite element method and concluded that for boreholes with different eccentricities, the stress concentration factor at the breakout tip becomes the same in the last step of expansion.

But in general, shear failure can occur in different planes depending on the values of local stresses. Figure 2 shows the different planes and the stress on them for an element around the borehole.

out (wide breakout) is created in horizontal planes ($r - \theta$ planes) perpendicular to the axis of the borehole, provided that $\sigma_r \leq \sigma_z \leq \sigma_\theta$. Shear failure can occur in $r - z$ planes provided that $\sigma_r \leq \sigma_\theta \leq \sigma_z$, this type of breakout is known as shallow knockout (Zang & Stephansson, 2010), and if $\sigma_\theta \leq \sigma_r \leq \sigma_z$, shear failure occur in the $z - \theta$ plane, which are known as high angle en-echelon cracks (Zang & Stephansson, 2010) (Table 1).

Two-dimensional analysis of borehole breakouts with the assumption of plane strain, due to not considering different stress planes, only and necessarily examine the failure in the $r - \theta$ plane, but in the field, breakout can be caused by failure in any of the stress planes, however, the final failure shape observed in the planes perpendicular to the borehole axis may still be V-shaped.

Al-Ajmi and Zimmerman (2006a), using a three-dimensional analytical model, observed that the Mohr-Coulomb failure criterion is too conservative in estimating the critical pressure required for stability of non-vertical boreholes, due to ignoring the strengthening effect of the principal intermediate stress.

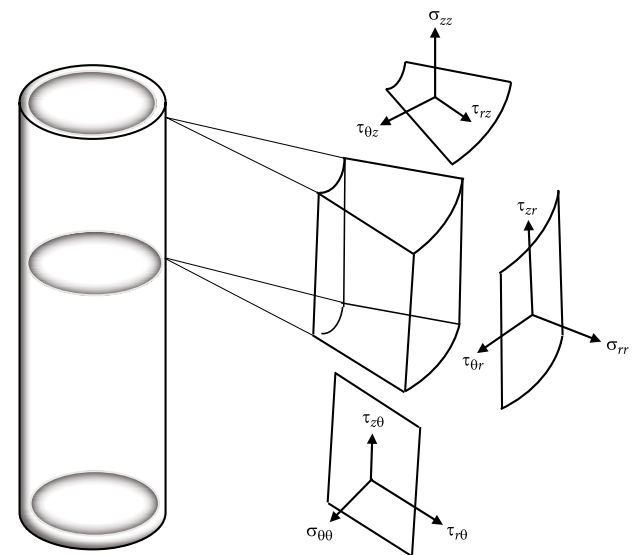


Figure 2. Stress on different plane around the borehole

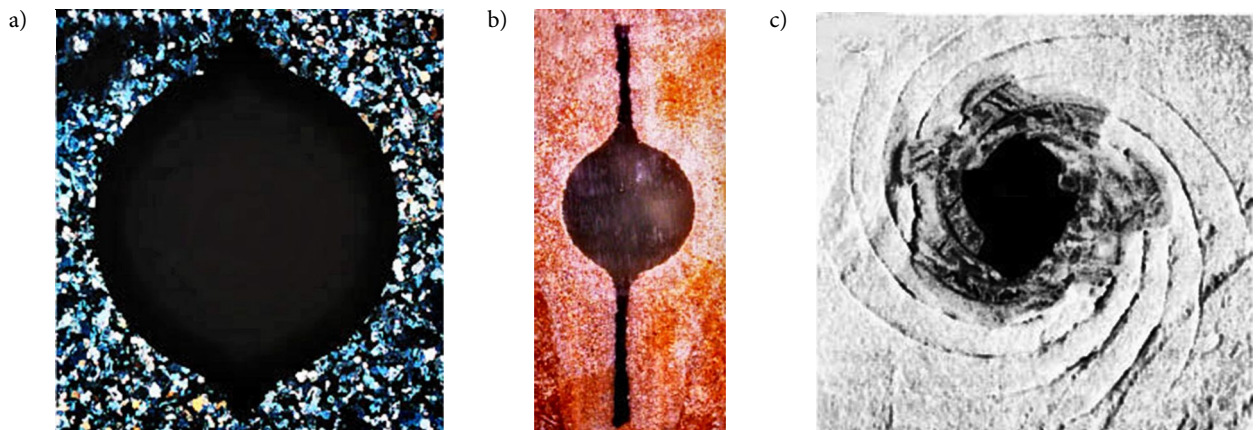
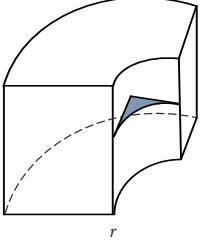
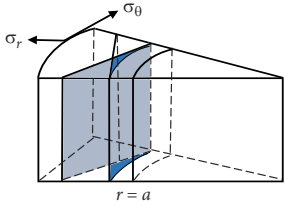
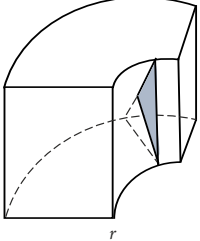
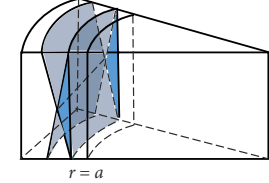
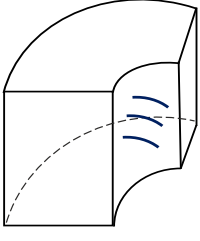
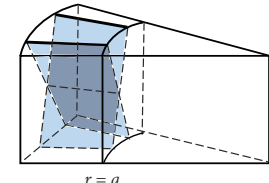


Figure 1. Breakouts: a) V-shaped (Haimson, 2007); b) slot shaped (Haimson & Lee, 2004); c) spiral shaped (Cerasi et al., 2005)

Table 1. Stress conditions and different forms of breakout: a) wide breakout; b) shallow knockout; c) high angle en-echelon cracks (Zang & Stephansson, 2010)

View from inside the borehole	Stress conditions	View from outside the borehole
	wide breakout $\sigma_r \leq \sigma_z \leq \sigma_\theta$	
	shallow knockout $\sigma_r \leq \sigma_\theta \leq \sigma_z$	
	high angle en-echelon cracks $\sigma_\theta \leq \sigma_r \leq \sigma_z$	

Using a simple analytical model, and Mohr-Coulomb, Mogi-Coulomb, Modified Lade and Tresca failure criteria, Manshad et al. (2014) obtained the optimum drilling direction and mud pressure.

Li et al. (2019) investigated the breakout in deviated wells using the finite element method and ABAQUS software. The results obtained from their analysis show that the well inclination has a great effect on the shape of the breakout and mud cake can reduce the extent of the breakout.

Another effective factor in breakout dimensions is the stress regime in the ground. If σ_v is the vertical principal in situ stress and σ_h is the minimum horizontal principal in situ stress and σ_H is the maximum horizontal principal in situ stress, the order of magnitude of these stresses may create three different stress regimes. The regime in which $\sigma_h < \sigma_H < \sigma_v$ is the normal faulting stress regime, and if $\sigma_h < \sigma_v < \sigma_H$ is the strike-slip faulting stress regime, and if $\sigma_v < \sigma_h < \sigma_H$ is the reverse faulting stress regime. What has often been of interest in previous breakout studies has been the strike-slip faulting stress regime.

Another limitation of previous studies was that they often considered the borehole vertically, while oriented and horizontal boreholes are very important in geomechanics and drilling industry. Oriented and horizontal boreholes in oil and gas fields increase the drainage area, this improves drilling and production efficiency. In some

cases, boreholes are drilled horizontally, so that distant locations can be accessed from the drilling site. Therefore, the investigation of shear stability around oriented boreholes is very important.

The purpose of this article is to provide an analytical model to investigate breakouts in oriented boreholes. In the presented analytical model, three important parameters are examined simultaneously; borehole orientation angle, different stress regimes and different failure planes. This model assumes linear elastic behavior, and the failure criterion of materials is based on Mogi-Coulomb criterion. Since the borehole is deviated with respect to the vertical, the analytical model is capable of three-dimensional analysis of all points around the borehole, but the failure shape is shown in the plane perpendicular to the borehole axis.

1. Problem definition

According to Figure 3, a deviated borehole is considered with anisotropic in situ stress; vertical stress σ_v , and the major and minor horizontal principal stresses σ_H and σ_h , respectively. Borehole drilling disrupts the initial stress distribution in the environment, especially around the borehole, so that in some points, the concentration of compressive stress and in some points, the concentration of tensile stress occurs. Failure occurs if the stress con-

centration exceeds the compressive or tensile strength of the rock in accordance with the selected failure criterion. The breakout shear failure zone develops along the smaller principal stress that has the highest stress concentration. The work steps are as follows: First, local stresses must be calculated at all points around the borehole. Then, using local stresses, principal stresses should be calculated. And in the last step, by substituting the principal stresses in the failure criteria for each point, it is controlled whether that point will fail or not. Because the borehole is diagonal and the model is three-dimensional, all nine components of the stress matrix are non-zero for any arbitrary point, and therefore there are three non-identical principal stresses ($\sigma_1, \sigma_2, \sigma_3$). For this reason, it is better to use the failure criterion in which the effect of the intermediate principal stress (σ_2) is also present. There are several failure criteria in which the effect of the intermediate principal stress is included (Lakirouhani & Hasanzadehshooili, 2011), such as Modified Lade failure criterion, Modified Wiebols-Cook criterion, Drucker-Prager failure criterion, and the Mogi-Coulomb failure criterion (Al-Ajmi & Zimmerman, 2006b). However, in this article, Mogi-Coulomb failure criterion is used to investigate shear or tensile failure in the rock surrounding the borehole. Although the present model examines the failure according to the coordinates of each point in the cylindrical coordinate system (r, θ, z) and is able to show the failure area in three dimensions, but for simplicity, the failure is only shown in the (r, θ) plane, which is perpendicular to the borehole axis. But it should be noted that the failure area shown includes failure in all planes, and this is the main difference between this model and the previous models and is the innovation of this article. The limitation of the analytical model presented in this article is that it obtains the failure area in the first stage of the breakout and cannot predict the progress of the breakout in the next steps. Figure 4 schematically shows the failure zone around the borehole in the (r, θ) plane. The failure zone has two characteristics, depth and width. Failure depth is the distance from the center of the borehole to the maximum depth of the failure zone, denoted by r_d , and the failure width, represented by θ_d is the central angle of the failure zone arc.

In the next section, stress transformation and stress distribution relationships around the borehole are presented. Then the equation of Mogi-Coulomb failure criterion is given. In Section 4 the calculation algorithm is presented. Section 5 presents the validation of the analytical model and computational algorithm using the results of breakout tests on Westerly granite. The final section of the article is related to the results of the analysis performed for different borehole orientation angles.

2. Stress transformation and stress distribution around the borehole

According to Figure 3 it is assumed that the in situ stresses ($\sigma_v, \sigma_h, \sigma_H$) define the (x', y', z') coordinate system; σ_v to be parallel to z' , σ_H to be parallel to x' and σ_h to be

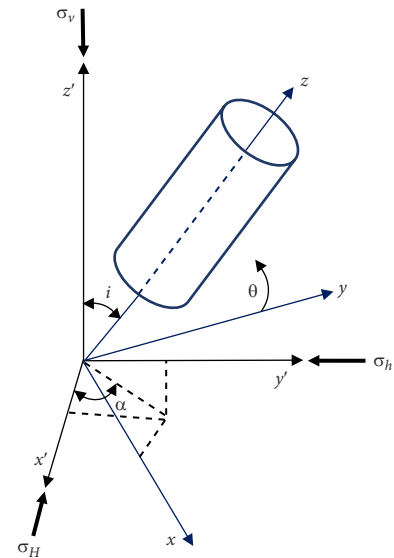


Figure 3. Coordinate system for a deviated borehole

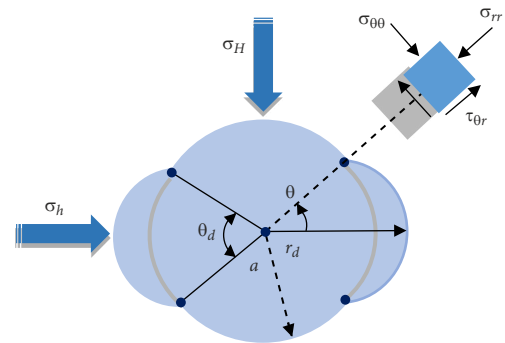


Figure 4. Schematic figure of borehole cross-section and failure zone on $r - \theta$ plane

parallel to y' . Another local coordinate system (x, y, z) is considered where z is along the borehole axis. In order to obtain the stress around the borehole, it is first necessary to determine the field stress in the local coordinate system.

If i is the angle between the z' -axis and the z -axis, and α is the angle between the x' -axis and the projection of the x -axis in the $x' - y'$ plane, then the transformation of the in situ stresses from the global coordinate system to the local coordinate system is carried out by the following transformation matrix (Valkó & Economides, 1995):

$$A = \begin{bmatrix} \cos \alpha \cos i & \sin \alpha \cos i & -\sin i \\ -\sin \alpha & \cos \alpha & 0 \\ \cos \alpha \sin i & \sin \alpha \sin i & \cos i \end{bmatrix}. \quad (1)$$

By using this transformation matrix, the local field stresses for the deviated borehole are given by:

$$\sigma_x^l = (\cos^2 \alpha \cos^2 i) \sigma_H + (\sin^2 \alpha \cos^2 i) \sigma_h + (\sin^2 i) \sigma_v; \quad (2)$$

$$\sigma_y^l = (\sin^2 \alpha) \sigma_H + (\cos^2 \alpha) \sigma_h; \quad (3)$$

$$\sigma_z^l = (\cos^2 \alpha \sin^2 i) \sigma_H + (\sin^2 \alpha \sin^2 i) \sigma_h + (\cos^2 i) \sigma_v; \quad (4)$$

$$\tau_{xy} = (-\cos \alpha \cos i \sin i) \sigma_H + (\sin \alpha \cos i \cos \alpha) \sigma_h; \quad (5)$$

$$\tau_{yz}^l = (-\sin \alpha \cos \alpha \sin i) \sigma_H + (\cos \alpha \sin \alpha \sin i) \sigma_h; \quad (6)$$

$$\tau_{zx}^l = (\cos^2 \alpha \sin i \cos i) \sigma_H + (\sin^2 \alpha \cos i \sin i) \sigma_h + (\cos i \sin i) \sigma_v. \quad (7)$$

The superscript l refers to local field stresses, and $i = 0^\circ$ means that the borehole is vertical. Now the distribution of stress around the borehole based on local stress is as follows (Valkó & Economides, 1995):

$$\begin{aligned} \sigma_r &= \frac{\sigma_x^l + \sigma_y^l}{2} \left(1 - \frac{a^2}{r^2} \right) - \\ &\frac{\sigma_x^l - \sigma_y^l}{2} \left(1 + 3 \frac{a^4}{r^4} - 4 \frac{a^2}{r^2} \right) \cos 2\theta - \\ &\tau_{xy}^l \left(1 + 3 \frac{a^4}{r^4} - 4 \frac{a^2}{r^2} \right) \sin 2\theta + p_w \frac{a^2}{r^2}; \end{aligned} \quad (8)$$

$$\begin{aligned} \sigma_\theta &= \frac{\sigma_x^l + \sigma_y^l}{2} \left(1 + \frac{a^2}{r^2} \right) + \\ &\frac{\sigma_x^l - \sigma_y^l}{2} \left(1 + 3 \frac{a^4}{r^4} \right) \cos 2\theta + \\ &\tau_{xy}^l \left(1 + 3 \frac{a^4}{r^4} \right) \sin 2\theta - p_w \frac{a^2}{r^2}; \end{aligned} \quad (9)$$

$$\begin{aligned} \sigma_z &= \sigma_z^l + \nu \left[2(\sigma_x^l - \sigma_y^l) \frac{a^2}{r^2} \cos 2\theta + \right. \\ &\left. 4\tau_{xy}^l \frac{a^2}{r^2} \sin 2\theta \right]; \end{aligned} \quad (10)$$

$$\begin{aligned} \tau_{r\theta} &= \frac{\sigma_x^l - \sigma_y^l}{2} \left(1 - 3 \frac{a^4}{r^4} + 2 \frac{a^2}{r^2} \right) \sin 2\theta - \\ &\tau_{xy}^l \left(1 - 3 \frac{a^4}{r^4} + 2 \frac{a^2}{r^2} \right) \cos 2\theta; \end{aligned} \quad (11)$$

$$\tau_{\theta z} = -(\tau_{xz}^l \cos \theta + \tau_{yz}^l \sin \theta) \left(1 + \frac{a^2}{r^2} \right); \quad (12)$$

$$\tau_{rz} = (\tau_{xz}^l \sin \theta - \tau_{yz}^l \cos \theta) \left(1 - \frac{a^2}{r^2} \right), \quad (13)$$

where r is the distance of the point from the borehole axis and θ the azimuth angle relative to the y -axis, a is the borehole radius and z is the position along the borehole axis.

3. Failure criterion

The Mogi-Coulomb failure criterion is defined as follows (Al-Ajmi & Zimmerman, 2006b):

$$\tau_{oct} = a + b\sigma_{m,2}; \quad (14)$$

$$\sigma_{m,2} = \frac{(\sigma_1 + \sigma_3)}{2}, \quad (15)$$

where

$$\tau_{oct} = \frac{1}{3} \sqrt{(\sigma_1 - \sigma_2)^2 + (\sigma_2 - \sigma_3)^2 + (\sigma_3 - \sigma_1)^2}, \quad (16)$$

parameters a and b are dependent on the mechanical properties of the rock materials as:

$$a = \frac{2\sqrt{2}}{3} \left(\frac{\sigma_c}{q+1} \right); \quad (17)$$

$$b = \frac{2\sqrt{2}}{3} \left(\frac{q-1}{q+1} \right), \quad (18)$$

where:

$$\sigma_c = \frac{2c \cos \phi}{1 - \sin \phi}; \quad (19)$$

$$q = \frac{1 + \sin \phi}{1 - \sin \phi} = \tan^2 \left(45 + \frac{\phi}{2} \right), \quad (20)$$

where c and ϕ are the cohesion and internal friction angle of the rock, respectively. Thus, failure function (F_{MG}) for this criterion is defined as:

$$F_{MG} = \frac{\tau_{oct}}{a + b\sigma_{m,2}}. \quad (21)$$

For any arbitrary point, failure occurs if $F_{MG} > 1$.

4. Calculation algorithm

Figure 5 shows the calculation algorithm based on the calculation steps mentioned in Section 1 and the relationships presented in Sections 2 and 3. The inputs of the problem include the mechanical properties of the rock

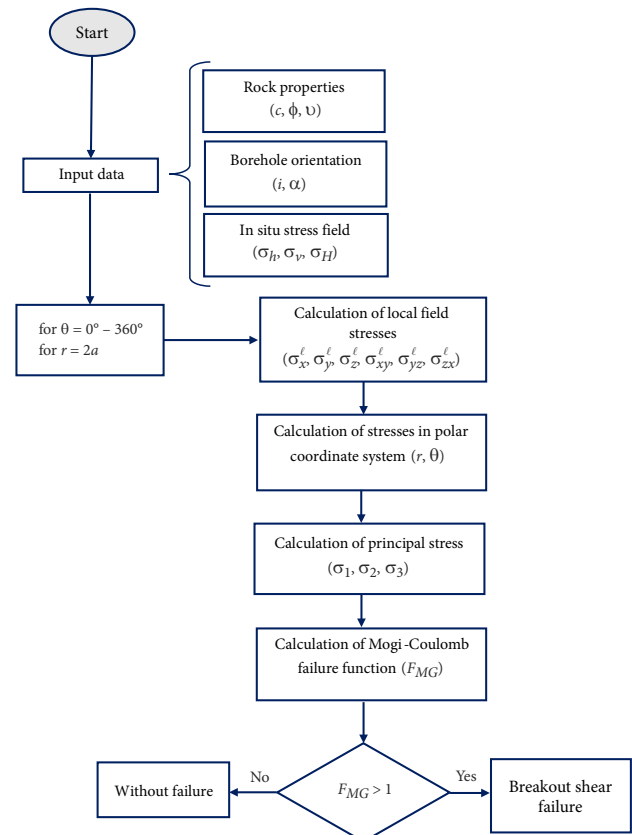


Figure 5. Calculation algorithm

materials, the deviation angle of the borehole and the in situ stress field in the initial coordinate system. The calculation steps are presented in the algorithm. The depth (z) is not directly observed in the relations, but it has an effect indirectly through the vertical stress (σ_v). In other words, the vertical stress cannot have a constant value and increases with increasing depth. But in this article, the analysis were done for a constant depth, and therefore the vertical stress is considered constant for each of the analyses. At each section, calculations are made for $\theta = 0^\circ - 360^\circ$ and the maximum radius equal to $2a$. Often the radius of the failure zone is less than $2a$.

By using the calculation algorithm and performing calculations for each point, according to the in situ stress field, the mechanical properties of the rock, the orientation angle of the borehole, the location of the point with respect to the borehole axis, and the failure criterion, it is determined whether that point has failed or not. To perform calculations, a computer program is coded in MATLAB software. In the next sections, validation and results are given.

5. Validation and comparison with laboratory results

In this section, a comparison is made between the results of laboratory studies conducted on Westerly granite (Song, 1998) with the analysis performed by the analytical model proposed in this article. Westerly granite is a crystalline rock with elastic, homogeneous and isotropic behavior, which is why it is often used in laboratory studies. Triaxial tests performed on Westerly granite samples have shown that $c = 28.7$ MPa and $\phi = 56.9^\circ$ for this rock (Song, 1998). For comparison, the normalized depth (r_d/a) and width (θ_d) of the failure zone shown in Figure 4 are used. The comparison results for different combinations of in situ stresses are given in Table 2 and it can be seen that the absolute error between r_d/a obtained from the laboratory model and the analytical model is a maximum of 0.165, and the absolute error for the breakout width (θ_d) is 6.88° at most. The width of the failure obtained from the analytical model is slightly more than the width of the laboratory model and the depth of the failure in the analytical model is slightly less than the laboratory model. In other

words, the failure zone in the laboratory model is narrower and deeper than the failure zone in the analytical model.

This difference can be related to the impact of the rock microstructure on the breakout dimensions, which is not considered in the analytical model, but will definitely be effective in the laboratory model. The difference between the two models can also be related to the size effect in the laboratory samples. Westerly granite laboratory samples were $11 \text{ cm} \times 11 \text{ cm} \times 11 \text{ cm}$ blocks with a hole of radius 2.23 cm in their center (Song, 1998). In various laboratory studies, the effect of hole diameter on breakout dimensions has been investigated, but the analytical model presented in this article uses the assumption of linear elastic behavior for materials and therefore is not able to investigate the size effect.

6. Results

The results of the analysis are given in this section. The properties of rock materials in the analysis of this section are as: $c = 25$ MPa, $\phi = 32.5^\circ$, $\nu = 0.25$. Because the borehole is diagonal and there is also the influence of the intermediate principal stress in the failure criterion, the analysis of this section has been performed for three different stress regimes; strike-slip faulting stress regime, normal faulting stress regime and reverse faulting stress regime, the results of which are given below. For each stress regime, the analysis has been done for two angles $\alpha = 0^\circ$ and $\alpha = 90^\circ$, in each case i between 0° to 90° has been varied with steps of 5° . According to Figure 3 and Figure 6a, $\alpha = 0^\circ$ means that the rotation of the borehole with the change of i occurs in the $\sigma_v - \sigma_H$ plane and around the axis σ_h and also $\alpha = 90^\circ$ means that the rotation of the borehole occurs, in the $\sigma_v - \sigma_h$ plane and around the axis σ_H (Figure 3, Figure 6b). In the following, for each stress regime, the results for two states $\alpha = 0^\circ$ and $\alpha = 90^\circ$ are given separately.

6.1. Results for the strike-slip faulting stress regime

The strike-slip faulting stress regime is the stress regime in which $\sigma_h < \sigma_v < \sigma_H$. To perform the analysis in this stress regime, the in situ stresses are selected as: $\sigma_h = 20$ MPa, $\sigma_v = 30$ MPa, $\sigma_H = 20$ MPa.

Table 2. Comparison between normalized failure depth (r_d/a) and width obtained from analytical model and laboratory model

Test No.	σ_h (MPa)	σ_v (MPa)	σ_H (MPa)	r_d/a			θ_d ($^\circ$)		
				Analytical model	Laboratory model	Absolute Error	Analytical model	Laboratory model	Absolute Error
1	20	40	160	1.2	1.260	0.06	44.88	42.44	2.44
2	20	40	180	1.235	1.268	0.033	47.08	42.62	4.46
3	20	40	200	1.265	1.283	0.018	48.98	46.11	2.87
4	20	60	180	1.24	1.242	0.002	47.8	40.92	6.88
5	20	60	200	1.26	1.287	0.027	48.86	44.82	4.04
6	40	60	180	1.085	1.139	0.054	32.22	30.88	1.34
7	40	60	200	1.115	1.280	0.165	36.26	39.68	3.42

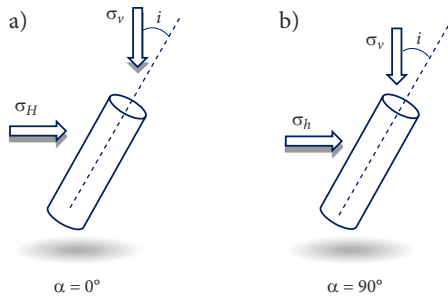


Figure 6. Oriented borehole and in situ stresses conditions: a) $\alpha = 0^\circ$ and b) $\alpha = 90^\circ$

The results in this case are given in Figures 7 and 8. Figure 7 shows the normalized failure depth (r_d/a) versus orientation angle (i) for $\alpha = 0^\circ$ (blue curve) and $\alpha = 90^\circ$ (red curve), and Figure 8 shows the failure width (θ_d) versus orientation angle (i) for $\alpha = 0^\circ$ (blue curve) and $\alpha = 90^\circ$ (red curve).

$\alpha = 0^\circ$: In this case, according to Figure 6a, the orientation angle is in the $\sigma_v - \sigma_H$ plane. It can be seen in Figures 7 and 8 when $\alpha = 0^\circ$, with the increase of orientation angle (i), the dimensions of the breakout shear failure area decrease, so that for $i > 70^\circ$, there is no breakout failure zone around the borehole. According to Figure 6a, as the ori-

entation angle of the borehole increases, the impact of the maximum principal stress on the borehole decreases, and in other words, the degree of local field stress anisotropy decreases, which makes the concentration of compressive stress on the borehole wall decrease, and as a result, the dimension of the breakout becomes smaller. In this case, the failure zone is formed along the minimum principal stress. Figure 9a shows the breakout shear failure contour for $\alpha = 0^\circ, i = 0^\circ$. In this case, tensile failure is also observed in the other two sides of the borehole wall. Contours are displayed in polar coordinates, where θ is the angle relative to the minimum principal stress.

$\alpha = 90^\circ$: In this case, the rotation angle is in the $\sigma_v - \sigma_h$ plane (Figure 6b). If $i = 0^\circ$, the dimensions of the breakout area are the same as the breakout area for $\alpha = 0^\circ, i = 0^\circ$, only rotated by 90° . But with the increase of the orientation angle of the borehole, the values of the depth and width of failure become different from the previous state, because the axis of the borehole rotates in the $\sigma_v - \sigma_h$ plane, which is different from the previous state. As can be seen in Figures 7 and 8, as the borehole orientation angle increases, the dimensions of the breakout zone increase, and this is due to the increase in compressive stress concentration. Figure 9b shows the failure contour in this condition ($\alpha = 90^\circ, i = 90^\circ$).

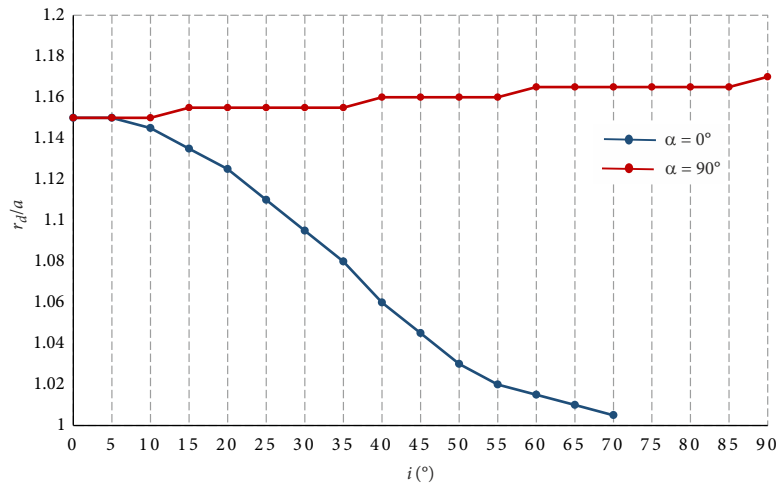


Figure 7. Normalized failure depth versus orientation angle for the strike-slip faulting stress regime

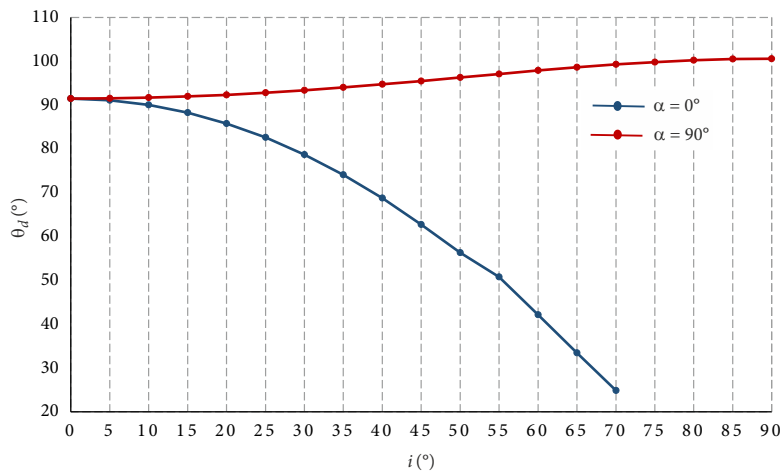


Figure 8. Failure width versus orientation angle for the strike-slip faulting stress regime

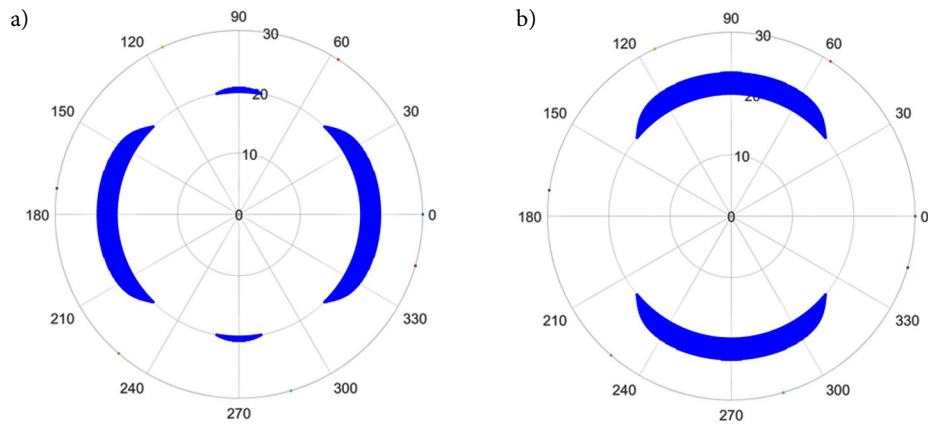


Figure 9. Failure contour for the strike-slip faulting stress regime: a) $\alpha = 0^\circ, i = 0^\circ$; b) $\alpha = 90^\circ, i = 90^\circ$

6.2. Results for the normal faulting stress regime

The normal faulting stress regime is the stress regime in which $\sigma_h < \sigma_H < \sigma_v$. Therefore, to perform the analysis in this regime, the in situ stresses have been selected as follows: $\sigma_h = 20$ MPa, $\sigma_H = 80$ MPa, $\sigma_v = 100$ MPa. The results of the analysis are presented in Figures 10 to 12.

$\alpha = 0^\circ$: In this case, with the increase of the orientation angle of the borehole, the depth of the breakout area gradually increases (blue curve, Figure 10), but the width of the breakout increases up to $i = 30^\circ$ and after that, it decreases at a very low rate (blue curve, Figure 11). An example of failure contour is shown in Figure 12a.

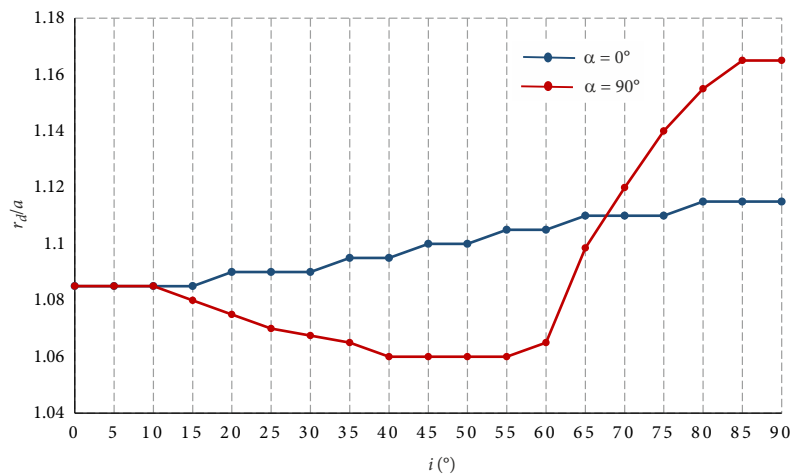


Figure 10. Normalized failure depth versus orientation angle for the normal faulting stress regime

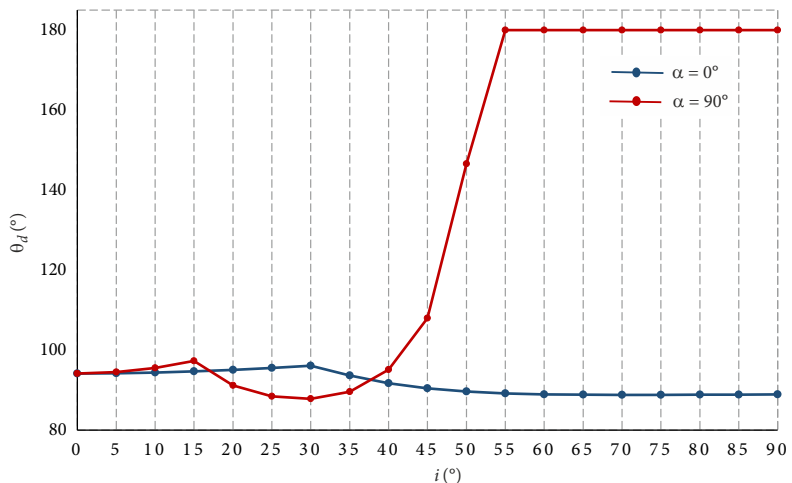


Figure 11. Failure width versus orientation angle for the normal faulting stress regime

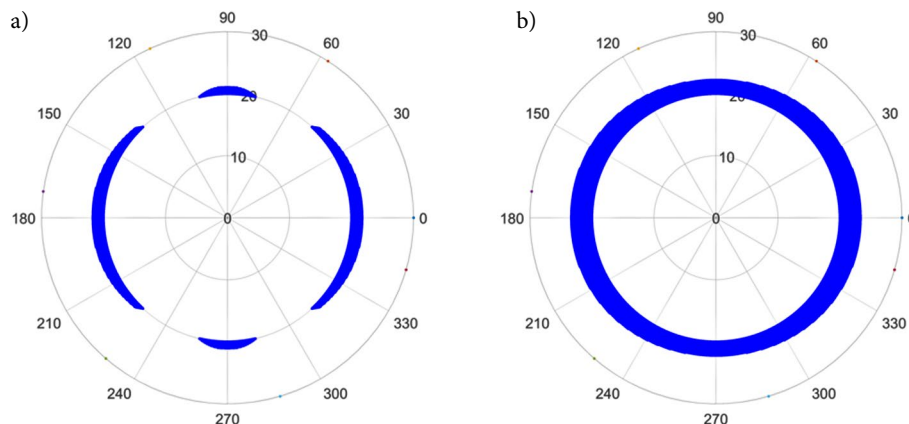


Figure 12. Failure contour for the normal faulting stress regime: a) $\alpha = 0^\circ, i = 0^\circ$; b) $\alpha = 90^\circ, i = 90^\circ$

$\alpha = 90^\circ$: In this situation, the depth of the breakout failure zone decreases with the increase of the borehole orientation angle from $i = 0^\circ$ to $i = 55^\circ$, but then it increases at a high rate (red curve, Figure 10). The remarkable thing that can be obtained from Figure 11 is that from $i = 30^\circ$ to $i = 55^\circ$, the failure width angle increases, so that at $i = 55^\circ$ the failure width is equal to 180° , that is, the entire borehole wall undergoes shear failure. The failure contour for this situation is shown in Figure 12b.

6.3. Results for the reverse faulting stress regime

The reverse faulting stress regime is the stress regime in which $\sigma_v < \sigma_h < \sigma_H$. To create this stress regime, the in situ stresses have been selected as follows: $\sigma_v = 20$ MPa, $\sigma_h = 50$ MPa, $\sigma_H = 100$ MPa. The results of the analysis are given in Figures 13 to 15.

$\alpha = 0^\circ$: In this case, by increasing the orientation angle of the borehole, the depth and width of the breakout

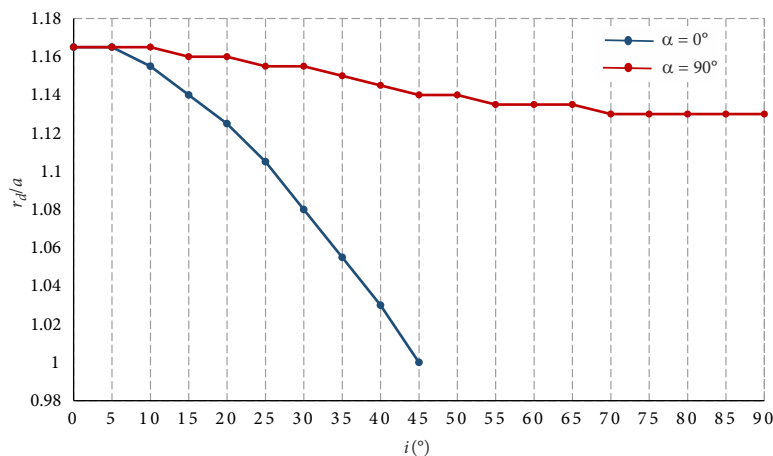


Figure 13. Normalized failure depth versus orientation angle for the reverse faulting stress regime

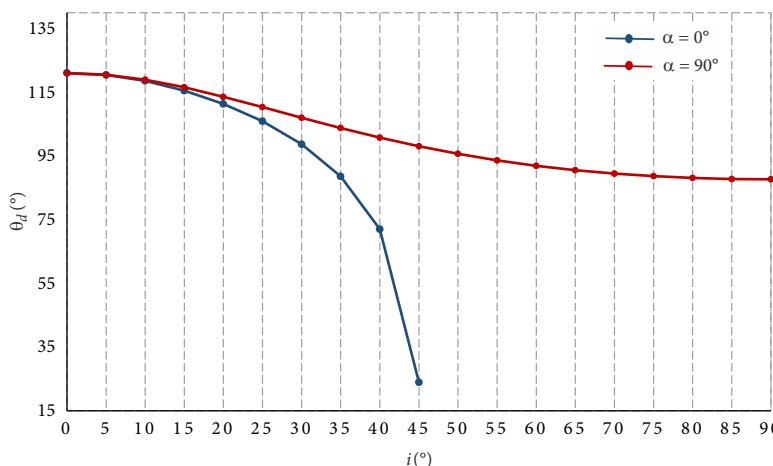


Figure 14. Failure width versus orientation angle for the reverse faulting stress regime

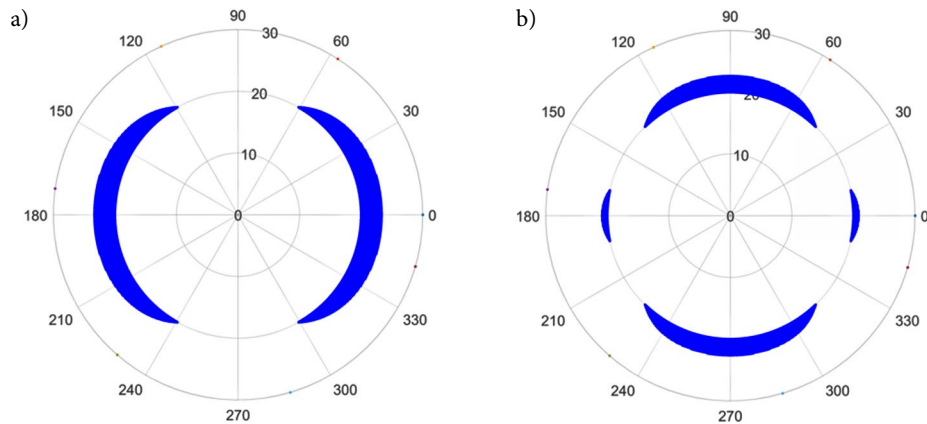


Figure 15. Failure contour for the reverse faulting stress regime: a) $\alpha = 0^\circ$, $i = 0^\circ$; b) $\alpha = 90^\circ$, $i = 90^\circ$

failure zone decreases and for $i > 45^\circ$, no failure zone is observed around the borehole (Figures 13 and 14). Figure 15a is related to the failure contour for $\alpha = 0^\circ$, $i = 0^\circ$.

$\alpha = 90^\circ$: This case is also similar to the previous case, that is, as the orientation angle of the borehole increases, the breakout dimensions decrease, but at a lower rate than the previous case. Figure 15b is related to the failure contour for $\alpha = 90^\circ$, $i = 90^\circ$.

Conclusions

Non-vertical, oriented and horizontal boreholes are drilled for many reasons. One of the important reasons for drilling oriented boreholes in oil fields is to improve drilling and production efficiency. Due to the action of shear and off-plane stresses, the dimensions of the breakout failure zone in oriented boreholes are different from their vertical counterparts.

In this article, an analytical model was presented to investigate shear failure caused by compressive stress or borehole breakout, around oriented boreholes. In this model, the stress distribution around the borehole was obtained based on the theory of elasticity, and the Mogi-Coulomb failure criterion was used for the failure criterion of rock materials, in which the effect of the intermediate principal stress is also present, and for this reason, it is suitable for the failure analysis around oriented boreholes. The presented analytical model was compared with the results of breakout tests on Westerly granite and it was observed that the absolute error between the two models is maximum 0.165 for the normalized depth of failure and maximum 6.88° for the failure width. To perform various analysis, a computer program was coded in MATLAB software. Because the stress regime is an influential factor in breakout dimensions, the analysis was performed in three different stress regimes; strike-slip faulting stress regime, normal faulting stress regime, and reverse faulting stress regime. Although breakout dimensions can be obtained in all directions using the model, for ease of comparison, breakout is only examined on the $r - \theta$ plane. Breakout dimensions on the $r - \theta$ plane mean the normalized depth of the breakout (r_d/a) and the width of the breakout (θ_d).

According to the results obtained:

1. In the strike-slip faulting stress regime ($\sigma_h < \sigma_v < \sigma_H$), when the orientation angle is in the $\sigma_v - \sigma_H$ plane ($\alpha = 0^\circ$), the dimensions of the breakout decrease with the increase of the orientation angle of the borehole. This is because by increasing the deviation angle of the borehole in this plane, the concentration of compressive stress on the wall of the borehole decreases and as a result the depth and width of the failure decreases. But in this stress regime, if the orientation angle is located in the $\sigma_v - \sigma_h$ plane ($\alpha = 90^\circ$), with the increase of the deviation angle of the borehole, the dimensions of the breakout increase, and this is due to the increase in the concentration of compressive stress on the wall of the borehole. In all cases, the breakout is formed along the minimum principal stress.
2. In the normal faulting stress regime, for $\alpha = 0^\circ$, the depth of the breakout increases with the increase of the deviation angle of the borehole, but the width of the breakout first increases and then decreases at a small rate. For $\alpha = 90^\circ$, as the deviation angle of the borehole increases, the width of the breakout increases until the shear failure of the breakout occurs in the entire wall of the borehole.
3. In the reverse faulting stress regime, in both cases $\alpha = 0^\circ$ and $\alpha = 90^\circ$, the depth and width of the breakout decreases with the increase of the deviation angle of the borehole.

In short, the orientation angle of the borehole and the stress regime are two important factors affecting the dimensions of the breakout and the stability or instability of the borehole. These two factors are sometimes synergistic with each other to create a breakout, and sometimes they are mutually exclusive. For example, it was seen that in the strike-slip faulting stress regime, if the orientation angle of the borehole is in the $\sigma_v - \sigma_H$ plane, the dimensions of the breakout in the oriented borehole are reduced compared to the vertical borehole, and if the orientation angle of the borehole is in the $\sigma_v - \sigma_h$ plane, the dimensions of the breakout compared to the vertical borehole, increase. Or, in the reverse faulting stress regime, whether the orienta-

tion angle of the borehole is in the $\sigma_v - \sigma_H$ plane or in the $\sigma_v - \sigma_h$ plane, the dimensions of the breakout in the oriented borehole are smaller than the breakout dimensions of the vertical borehole. Anyway, the ideal situation is that according to the stress regime, the orientation angle of the borehole is in the plane where the least shear instability occurs.

References

- Al-Ajmi, A., & Zimmerman, R. (2006a). *A new 3D stability model for the design of non-vertical wellbores* [Paper presentation]. The Golden Rocks 2006, The 41st U.S. Symposium on Rock Mechanics (USRMS), Colorado, USA.
- Al-Ajmi, A. M., & Zimmerman, R. W. (2006b). Stability analysis of vertical boreholes using the Mogi-Coulomb failure criterion. *International Journal of Rock Mechanics and Mining Sciences*, 43(8), 1200–1211. <https://doi.org/10.1016/j.ijrmms.2006.04.001>
- Bahrehdar, M., & Lakirouhani, A. (2022). Evaluation of the depth and width of progressive failure of breakout based on different failure criteria, using a finite element numerical model. *Arabian Journal for Science and Engineering*, 47, 11825–11839. <https://doi.org/10.1007/s13369-022-06640-9>
- Bahrehdar, M., & Lakirouhani, A. (2023). Effect of eccentricity on breakout propagation around noncircular boreholes. *Advances in Civil Engineering*, 2023, 6962648. <https://doi.org/10.1155/2023/6962648>
- Bell, J. S., & Gough, D. I. (1979). Northeast-southwest compressive stress in Alberta evidence from oil wells. *Earth and Planetary Science Letters*, 45(2), 475–482. [https://doi.org/10.1016/0012-821X\(79\)90146-8](https://doi.org/10.1016/0012-821X(79)90146-8)
- Cerasi, P., Papamichos, E., & Stenebråten, J. F. (2005). Quantitative sand-production prediction: Friction-dominated flow model. In *SPE Latin American and Caribbean Petroleum Engineering Conference* (No. SPE-94791-MS), Rio de Janeiro, Brazil. <https://doi.org/10.2118/94791-MS>
- Cook, B. K., Lee, M. Y., DiGiovanni, A. A., Bronowski, D. R., Perkins, E. D., & Williams, J. R. (2004). Discrete element modeling applied to laboratory simulation of near-wellbore mechanics. *International Journal of Geomechanics*, 4(1), 19–27. [https://doi.org/10.1061/\(ASCE\)1532-3641\(2004\)4:1\(19\)](https://doi.org/10.1061/(ASCE)1532-3641(2004)4:1(19))
- Cuss, R. J., Rutter, E. H., & Holloway, R. F. (2003). Experimental observations of the mechanics of borehole failure in porous sandstone. *International Journal of Rock Mechanics and Mining Sciences*, 40(5), 747–761. [https://doi.org/10.1016/S1365-1609\(03\)00068-6](https://doi.org/10.1016/S1365-1609(03)00068-6)
- Ewy, R. T., & Cook, N. G. W. (1990). Deformation and fracture around cylindrical openings in rock – I. Observations and analysis of deformations. *International Journal of Rock Mechanics and Mining Sciences & Geomechanics Abstracts*, 27(5), 387–407. [https://doi.org/10.1016/0148-9062\(90\)92713-O](https://doi.org/10.1016/0148-9062(90)92713-O)
- Gough, D. I., & Bell, J. S. (1982). Stress orientations from borehole wall fractures with examples from Colorado, East Texas, and Northern Canada. *Canadian Journal of Earth Sciences*, 19(7), 1358–1370. <https://doi.org/10.1139/e82-118>
- Haimson, B. (2007). Micromechanisms of borehole instability leading to breakouts in rocks. *International Journal of Rock Mechanics and Mining Sciences*, 44(2), 157–173. <https://doi.org/10.1016/j.ijrmms.2006.06.002>
- Haimson, B. C., & Herrick, C. G. (1986). Borehole breakouts—a new tool for estimating in situ stress?. In *Proceedings of the International Symposium on Rock Stress and Rock Stress Measurements* (pp. 271–280), Stockholm, Sweden.
- Haimson, B., & Kovacich, J. (2003). Borehole instability in high-porosity Berea sandstone and factors affecting dimensions and shape of fracture-like breakouts. *Engineering Geology*, 69(3), 219–231. [https://doi.org/10.1016/S0013-7952\(02\)00283-1](https://doi.org/10.1016/S0013-7952(02)00283-1)
- Haimson, B., & Lee, H. (2004). Borehole breakouts and compaction bands in two high-porosity sandstones. *International Journal of Rock Mechanics and Mining Sciences*, 41(2), 287–301. <https://doi.org/10.1016/j.ijrmms.2003.09.001>
- Haimson, B. C., & Song, I. (1993). Laboratory study of borehole breakouts in Cordova Cream: a case of shear failure mechanism. *International Journal of Rock Mechanics and Mining Sciences & Geomechanics Abstracts*, 30(9), 1047–1056. [https://doi.org/10.1016/0148-9062\(93\)90070-T](https://doi.org/10.1016/0148-9062(93)90070-T)
- Haimson, B. C., & Song, I. (1998). Borehole breakouts in Berea sandstone: Two porosity-dependent distinct shapes and mechanisms of formation. In *The SPE/ISRM Rock Mechanics in Petroleum Engineering* (No. SPE-47249-MS), Trondheim, Norway. <https://doi.org/10.2118/47249-MS>
- Herrick, C. G., & Haimson, B. C. (1994). Modeling of episodic failure leading to borehole breakouts in Alabama limestone. In *Proceedings of the 1st North American Rock Mechanics Symposium, Rock Mechanics: Models and measurements* (pp. 217–224). Balkema, Austin, Rotterdam.
- Hickman, S. H., Healy, J. H., & Zoback, M. D. (1985). In situ stress, natural fracture distribution, and borehole elongation in the Auburn Geothermal Well, Auburn, New York. *Journal of Geophysical Research*, 90(B7), 5497–5512. <https://doi.org/10.1029/JB090iB07p05497>
- Jolfaei, S., & Lakirouhani, A. (2022). Sensitivity analysis of effective parameters in borehole failure, using neural network. *Advances in Civil Engineering*, 2022, 4958004. <https://doi.org/10.1155/2022/4958004>
- Klaetsch, A. R., & Haimson, B. C. (2002). Porosity-dependent fracture-like breakouts in St. Peter sandstone. In R. Hammah, W. Bawden, J. Curran, & M. Telesnicki (Eds.), *Proceedings of the 5th NARMS-TAC Conference. Mining and tunneling: innovation and opportunity* (pp. 1365–1371). University of Toronto, Toronto, Canada.
- Lakirouhani, A., Bahrehdar, M., Medzvieckas, J., & Kliukas, R. (2021). Comparison of predicted failure area around the boreholes in the strike-slip faulting stress regime with Hoek-Brown and Fairhurst generalized criteria. *Journal of Civil Engineering and Management*, 27(5), 346–354. <https://doi.org/10.3846/jcem.2021.15020>
- Lakirouhani, A., & Hasanzadehshooiili, H. (2011). Review of rock strength criteria. In *Proceedings of the 22nd World Mining Congress & Expo* (pp. 473–482), Istanbul, Turkey.
- Lee, M., & Haimson, B. (1993). Laboratory study of borehole breakouts in Lac du Bonnet granite: A case of extensile failure mechanism. *International Journal of Rock Mechanics and Mining Sciences & Geomechanics Abstracts*, 30(7), 1039–1045. [https://doi.org/10.1016/0148-9062\(93\)90069-P](https://doi.org/10.1016/0148-9062(93)90069-P)
- Li, L., Papamichos, E., & Cerasi, P. (2006). Investigation of sand production mechanisms using DEM with fluid flow. In A. V. Cotthem, R. Charlier, J. F. Thimus, & J. P. Tshibangu (Eds.), *Eurock 2006: Multiphysics coupling and long term behaviour in rock mechanics: Proceedings of the International Symposium of the International Society for Rock Mechanics* (pp. 241–247). Taylor & Francis. <https://doi.org/10.1201/9781439833469.ch33>
- Li, X., El Mohtar, C. S., & Gray, K. E. (2019). 3D poro-elasto-plastic modeling of breakouts in deviated wells. *Journal of Petroleum Science and Engineering*, 174, 913–920. <https://doi.org/10.1016/j.petrol.2018.11.086>

- Manshad, A. K., Jalalifar, H., & Aslannejad, M. (2014). Analysis of vertical, horizontal and deviated wellbores stability by analytical and numerical methods. *Journal of Petroleum Exploration and Production Technology*, 4(4), 359–369.
<https://doi.org/10.1007/s13202-014-0100-7>
- Mastin, L. G. (1984). *The development of borehole breakouts in sandstone* [Doctoral dissertation]. Stanford University, California, USA.
- Meier, T., Rybacki, E., Reinicke, A., & Dresen, G. (2013). Influence of borehole diameter on the formation of borehole breakouts in black shale. *International Journal of Rock Mechanics and Mining Sciences*, 62, 74–85.
<https://doi.org/10.1016/j.ijrmms.2013.03.012>
- Papamichos, E. (1999). Sand production and well productivity in conventional reservoirs. In *Vail Rocks 1999, The 37th U.S. Symposium on Rock Mechanics (USRMS)* (No. ARMA-99-0209), Vail, Colorado, USA.
- Papamichos, E., Tronvoll, J., Skjærstein, A., & Unander, T. E. (2010). Hole stability of Red Wildmoor sandstone under anisotropic stresses and sand production criterion. *Journal of Petroleum Science and Engineering*, 72(1), 78–92.
<https://doi.org/10.1016/j.petrol.2010.03.006>
- Potyondy, D. O., & Cundall, P. A. (2004). A bonded-particle model for rock. *International Journal of Rock Mechanics and Mining Sciences*, 41(8), 1329–1364.
<https://doi.org/10.1016/j.ijrmms.2004.09.011>
- Rahmati, H., Nouri, A., Chan, D., & Vaziri, H. (2021). Relationship between rock macro-and micro-properties and wellbore breakout type. *Underground Space*, 6(1), 62–75.
<https://doi.org/10.1016/j.undsp.2019.10.001>
- Setiawan, N. B., & Zimmerman, R. W. (2022). Semi-analytical method for modeling wellbore breakout development. *Rock Mechanics and Rock Engineering*, 55(5), 2987–3000.
<https://doi.org/10.1007/s00603-022-02850-7>
- Shamir, G., & Zoback, M. D. (1992). Stress orientation profile to 3.5 km depth near the San Andreas Fault at Cajon Pass, California. *Journal of Geophysical Research: Solid Earth*, 97(B4), 5059–5080. <https://doi.org/10.1029/91JB02959>
- Song, I. (1998). *Borehole breakouts and core diskings in Westerly granite: Mechanisms of formation and relationship to in situ stress* [PhD thesis]. University of Wisconsin, Madison, USA.
- Tronvoll, J., & Fjær, E. (1994). Experimental study of sand production from perforation cavities. *International Journal of Rock Mechanics and Mining Sciences & Geomechanics Abstracts*, 31(5), 393–410.
[https://doi.org/10.1016/0148-9062\(94\)90144-9](https://doi.org/10.1016/0148-9062(94)90144-9)
- Valkó, P., & Economides, M. J. (1995). *Hydraulic fracture mechanics*. John Wiley & Sons.
- Van den Hoek, P. J. (2001). Prediction of different types of cavity failure using bifurcation theory. In *DC Rocks 2001, The 38th U.S. Symposium on Rock Mechanics (USRMS)* (No. ARMA-01-0045), Washington, D.C., USA.
- Zang, A., & Stephansson, O. (Eds.). (2010). *Stress field of the earth's crust*. Springer, Dordrecht, Heidelberg, New York.
<https://doi.org/10.1007/978-1-4020-8444-7>
- Zoback, M. D., Moos, D., Mastin, L., & Anderson, R. N. (1985). Wellbore breakouts and in situ stress. *Journal of Geophysical Research: Solid Earth*, 90(B7), 5523–5530.
<https://doi.org/10.1029/JB090iB07p05523>